Semi-analytical spatial derivative for adaptive mesh refinement

Érico Tenório França*, Ivaldevingles Rodrigues and Valdelírio da Silva e Silva, UFPA

This paper was prepared for presentation during the 18th International Congress of the Brazilian Geophysical Society held in Rio de Janeiro, Brazil, 16-19 October 2023.

Abstract

Geophysical modeling often requires the computation of spatial derivatives to obtain additional components of physical fields used in geophysical methods. In this paper, we propose a new approach to calculating spatial derivatives in a semi-analytical manner. The finite element method is employed to solve the underlying differential equations, which involves discretizing the domain and forming a linear system. The proposed semi-analytical spatial derivative is applied analytically to this linear system. In addition, mesh refinement is crucial for obtaining accurate solutions when working with discretized domains. To address this issue, we utilize an a posteriori error estimation method to generate an efficient mesh that produces accurate solutions. The semi-analytical spatial derivative is employed to define a new local error estimator within the refinement procedure. To validate the effectiveness of our approach, we apply the semi-analytical derivative and the refinement procedure to two differential equation problems. The first problem involves a simpler Poisson equation, which aids in visualization and understanding. The second problem focuses on the 2D modeling of the magnetotelluric method, where the solution and its spatial derivative are required for impedance calculations. In both cases, our proposed methodology demonstrates efficiency, particularly in the refinement procedure for modeling.

Introduction

Numerical derivative methods are widely used in various scientific and engineering applications, particularly in solving partial differential equations (PDEs) through finite element, finite difference, or spectral methods. These methods are employed to calculate the spatial derivatives of a solution field, which are critical in modeling and simulation processes.

We present a new approach to obtain spatial derivatives in a semi-analytical manner, applied to problems solved by the finite element method (FEM). As FEM is a numerical method to obtain the solution of PDEs through a linear system, the proposed procedure is analytically applied to this system. Newman (1997) presents a similar procedure to obtain the sensitivity matrix from the derivative of the linear system with respect to the parameters.

The validation of the semi-analytic derivative is carried out on a Poisson's equation problem, whose solution and spatial derivative are calculated analytically. Then, its application to the adaptive mesh refinement problem is proposed. Due to its nature, it is used in the recovery-based error estimation, a class within the a posteriori error method (Ainsworth & Oden, 2000; Grätsch & Bathe, 2005). In the works of Key & Weiss (2006) and Li & Key (2007), this methodology is applied to the modeling of electromagnetic methods. In these works, a dual or adjoint problem is used to quantify the local influence of non-local errors. We use a modified gradient obtained with the semi-analytical derivative procedure to locate and quantify the local influence, and then define a new local error estimator.

Finally, we apply an adaptive mesh refinement algorithm to the problem of the Poisson equation and to the modeling of the magnetotelluric (MT) method. In the latter, an optimization process is used in the adaptive refinement. The results of the proposed estimator are compared with the standard error estimator, and show efficiency in terms of the number of nodes.

Poisson's equation

In electrostatic field problems, the electric potential (ϕ) is governed by the two-dimensional Poisson equation (Jin, 2002),

$$-\nabla^2\phi = h \,, \tag{1}$$

where the potential source $h = \rho/\varepsilon$ is given by the ratio of the charge density (ρ) and the dielectric permittivity of the medium (ε). Considering a rectangular two-dimensional domain $\Omega = (0,2)\times(0,2)$, and $h(x,y)$ is chosen such that the analytical solution of equation 1 is given by,

$$\phi(x,y) = 10(1-e^{x})(1-e^{x-2})(1-e^{y})(1-e^{y-2}) \,, \tag{2}$$

whose values on the domain boundaries are zero.

Finite Element Method

The solution of equation 1 can be obtained via FEM. The Appendix presents the mathematical development of applying the Galerkin method to triangular elements, resulting in the elemental system $\mathbf{K}^e\mathbf{u}^e = \mathbf{g}^e$. Jin (2002) shows that the assembly of the global system is obtained by $\mathbf{K} = \sum_{e=1}^{M}\mathbf{K}^e$ and $\mathbf{g} = \sum_{e=1}^{M}\mathbf{g}^e$ (M number of elements). Thus, the solution of the electric potential ϕ in the domain $\Omega \subset \mathbb{R}^2$ is obtained from the following linear system:

$$\mathbf{K}\,\mathbf{u} = \mathbf{g} \,, \tag{3}$$

of size N (N number of nodes), where $\mathbf{u}$ is the solution vector containing the electric potential ϕ at all coordinates

$(\mathbf{x},\mathbf{y}) \subset \Omega$, $\mathbf{g}$ is the vector related to the physical laws describing the problem, referred to as the vector of nodal forces. The matrix $\mathbf{K}$ is directly linked to the problem geometry, referred to as the matrix stiffness, and it is sparse, symmetric, and positive definite. Figure 1 shows the analytical and FEM solutions (equation 1).

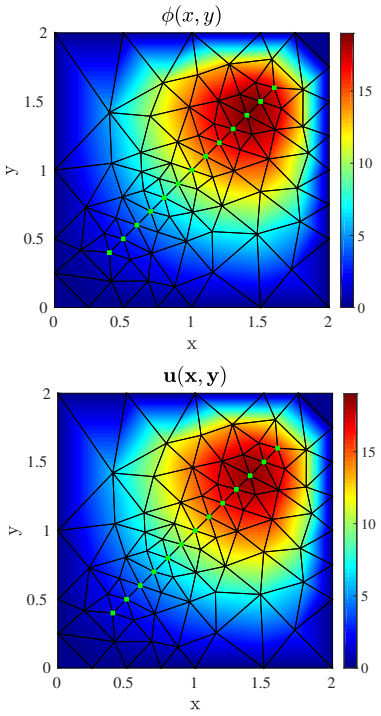

Figure 1 – Comparison between the analytical solution (ϕ) and the solution obtained via FEM ($\boldsymbol{u}$). Mesh with 87 nodes.

Semi-analytical spatial derivative

In this section, an approach is presented to obtain the spatial derivative of the linear system 3 in a semi-analytical manner. This procedure is similar to the one discussed in Newman & Alumbaugh (1997) for obtaining the sensitivity matrix, which involves taking derivatives of the linear system 3 with respect to the parameters. In this case, the elemental system $\mathbf{K}^e\mathbf{u}^e = \mathbf{g}^e$ is differentiated with respect to the coordinate x_n $(n = 1,2,3)$, where $x_n \in \mathbf{x}^e$. Therefore, we have:

$$\mathbf{K}^e \frac{\partial \mathbf{u}^e}{\partial x_n} = \frac{\partial \mathbf{g}^e}{\partial x_n} - \frac{\partial \mathbf{K}^e}{\partial x_n}\mathbf{u}^e, \tag{4}$$

where the matrix $\partial\mathbf{K}^e/\partial x_n$ and the vector $\partial\mathbf{g}^e/\partial x_n$ are, respectively,

$$\frac{\partial K^e_{ij}}{\partial x_n} = \frac{-1}{4A_e}\left[\frac{b_n}{2A_e}\,\mathrm{sgn}(B_e)(b_j b_i + c_j c_i) - \left(c_i\frac{\partial c_j}{\partial x_n} + c_j\frac{\partial c_i}{\partial x_n}\right)\right], \tag{5}$$

$$\frac{\partial g^e_i}{\partial x_n} = \frac{1}{12}\left[\frac{b_n}{2}\,\mathrm{sgn}(B_e)\sum_{j=1}^{3}(1+\delta(i-j))h_j + A_e\,\frac{\partial h_n}{\partial x_n}(1+\delta(i-n))\right], \tag{6}$$

where $i,j = 1,2,3$ and $B_e = \frac{1}{2}(a_1+a_2+a_3)$. The definitions of the variables above are presented in the Appendix. The derivative $\partial c_k/\partial x_n$ ($k = i$ or j) is given by,

$$\frac{\partial c_k}{\partial x_n} = \mathrm{sgn}(n-k)(-1)^{n+k-2}.$$

The system 4 shows that the derivatives with respect to the elements of the vector $\mathbf{x}^e$ result in 3 independent systems, which follow the following assembly of the global system,

$$\frac{\partial \mathbf{K}}{\partial \mathbf{x}} = \sum_{e=1}^{M}\sum_{n=1}^{3}\frac{\partial \mathbf{K}^e}{\partial x_n} \quad \text{and} \quad \frac{\partial \mathbf{g}}{\partial \mathbf{x}} = \sum_{e=1}^{M}\sum_{n=1}^{3}\frac{\partial \mathbf{g}^e}{\partial x_n},$$

thus, the global system is given by:

$$\mathbf{K}\frac{\partial \mathbf{u}}{\partial \mathbf{x}} = \frac{\partial \mathbf{g}}{\partial \mathbf{x}} - \frac{\partial \mathbf{K}}{\partial \mathbf{x}}\mathbf{u}, \tag{7}$$

whose Neumann boundary condition is applied using the values of $\partial\phi/\partial x$. Figure 2 shows the comparison between the analytical and the proposed semi-analytical derivatives.

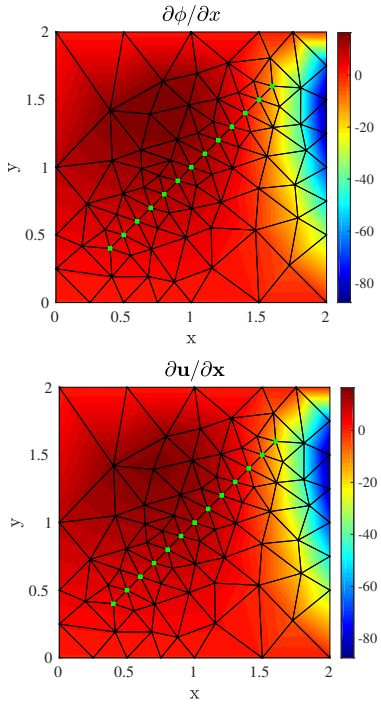

Figure 2 – Comparison between the analytical derivative ($\partial\phi/\partial x$) and the semi-analytical derivative ($\partial\boldsymbol{u}/\partial\boldsymbol{x}$). The values at the green points are shown in Figure 5.

Particular case

The system 7 is the general case where the spatial derivative of the solution is obtained for all coordinates in the domain Ω. Next, we will address the following particular case, where the spatial derivatives are obtained only at the coordinates $(\mathbf{x}^*,\mathbf{y}^*)$, where $(\mathbf{x}^*,\mathbf{y}^*) \subset (\mathbf{x},\mathbf{y})$. In other words, at some points of the discretization.

Figure 3 shows the point $P_i(x_i, y_i)$, where $P_i \in (\mathbf{x}^*, \mathbf{y}^*)$, and by taking the derivative of the elemental system with respect to x_i, we arrive at the system 4, since $x_i \in \mathbf{x}^e$. Thus, the derivatives

$$\frac{\partial \mathbf{K}^e}{\partial x_i} = \frac{\partial \mathbf{K}^e}{\partial x_n} \quad \text{and} \quad \frac{\partial \mathbf{g}^e}{\partial x_i} = \frac{\partial \mathbf{g}^e}{\partial x_n},$$

where n is the numbering within the elemental system ($n = 1$ to 3) for the coordinate x_i. Figure 3 shows elements 5, 23, and 27, where x_i changes the numbering n within each element. Therefore, the derivative of the matrix $\partial \mathbf{K}^5 / \partial x_i$ of element 5 will be with respect to x_2, while for elements 23 and 27, they will be with respect to x_1 and x_3, respectively.

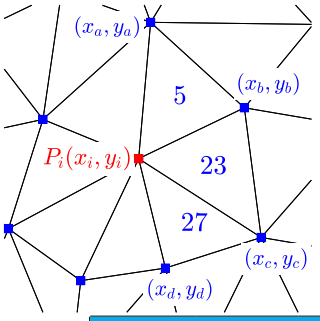

		Local numbering		
		1	2	3
Element	5	(x_a, y_a)	(x_i, y_i)	(x_b, y_b)
	23	(x_i, y_i)	(x_a, y_a)	(x_c, y_c)
	27	(x_d, y_d)	(x_b, y_b)	(x_i, y_i)

Figure 3 – Location of point $P(x_i, y_i)$ and the elements that share this point.

In this case, the system 4 results in a different global system than the general case, since the derivative is taken with respect to only one element of $\mathbf{x}^e$. Thus, the global system follows the following assembly,

$$\frac{\partial \mathbf{K}}{\partial \mathbf{x}^*} = \sum_{e=1}^{L} \frac{\partial \mathbf{K}^e}{\partial x_n} \quad \text{and} \quad \frac{\partial \mathbf{g}}{\partial \mathbf{x}^*} = \sum_{e=1}^{L} \frac{\partial \mathbf{g}^e}{\partial x_n},$$

where L is the number of elements that share the coordinates $(\mathbf{x}^*, \mathbf{y}^*)$ and n is the local numbering for each of these coordinates.

The global system for the particular case is similar to system 7 (with $\mathbf{x} = \mathbf{x}^*$), however, with a sparsity degree that depends on the number of elements in $(\mathbf{x}^*, \mathbf{y}^*)$. In addition, a homogeneous Neumann boundary condition is applied. A similar procedure is performed to obtain the derivatives $\partial \mathbf{u} / \partial \mathbf{y}$ and $\partial \mathbf{u} / \partial \mathbf{y}^*$.

Figure 4 shows the derivative $\partial \mathbf{u} / \partial \mathbf{x}^*$ for the set of positions $(\mathbf{x}^*, \mathbf{y}^*)$. The values of $\partial \mathbf{u} / \partial \mathbf{x}$ and $\partial \mathbf{u} / \partial \mathbf{x}^*$ at these positions are plotted in Figure 5, and we can observe a coherence of these values compared to the analytic derivative. Due to the coarse mesh, both the solution and the derivative of the solution are not accurate. To solve this problem, adaptive mesh refinement is performed.

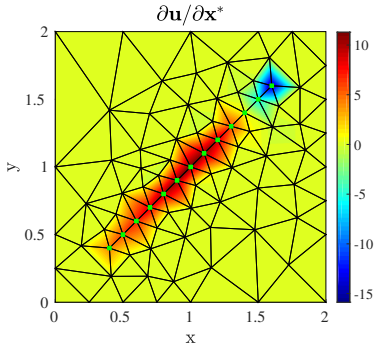

Figure 4 – Semi-analytical derivative $\partial \boldsymbol{u} / \partial \boldsymbol{x}^*$. The values at the green points represent the positions $(\boldsymbol{x}^*, \boldsymbol{y}^*)$.

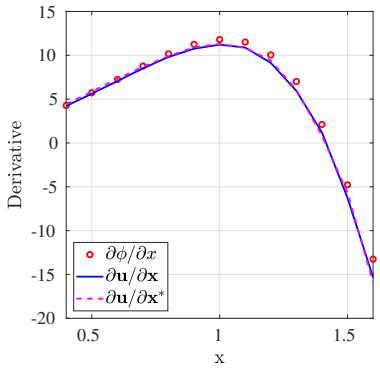

Figure 5 – Profile with values of the analytical and semi-analytical derivatives at coordinates $(\boldsymbol{x}^*, \boldsymbol{y}^*)$.

A posteriori error estimation

The posterior error estimation method is based on an evaluation of the numerical solution obtained by an approximation method, such as the FEM, to identify where the solution is not sufficiently accurate. Ainsworth & Oden (2000) discusses the theory and applications of posterior error estimation in finite element analysis.

Key & Weiss (2006) and Li & Key (2007) employ the recovery-based error estimation method, whose local error estimator is given by:

$$\eta_e = \|\nabla \widetilde{u}_h - \nabla u_h\|_{L_2(e)}, \tag{8}$$

where ∇u_h is the gradient of the approximate solution and $\nabla \widetilde{u}_h$ is the recovered gradient. Zienkiewicz & Zhu (1987) suggested post-processing the recovered gradient in terms of the interpolation functions $\nabla \widetilde{u}_h = \sum_{j=1}^{N} (\nabla \widetilde{u}_h)_j \varphi_j$. Thus, the recovered gradient is determined by a standard L_2 projection,

$$\int_\Omega \varphi_i (\nabla \widetilde{u}_h - \nabla u_h) \, d\Omega = 0 \quad i = 1, \ldots, N, \tag{9}$$

which leads to a linear system for determining the nodal values $(\nabla \widetilde{u}_h)_j$,

$$\sum_{j=1}^{N} \int_\Omega \varphi_i \varphi_j \, d\Omega \, (\nabla \widetilde{u}_h)_j = \int_\Omega \varphi_i \nabla u_h \, d\Omega \quad i = 1, \ldots, N. \tag{10}$$

Key & Weiss (2006) refers to the standard estimator as the basic error estimator (BEE), as it can be adapted to many numerical problems. Based on this, we present a new approach to the BEE, using the gradient of the approximate solution for the particular case $\nabla \mathbf{u}^* = \left(\frac{\partial \mathbf{u}}{\partial \mathbf{x}^*}, \frac{\partial \mathbf{u}}{\partial \mathbf{y}^*} \right)$. Thus, the new recovered gradient is obtained from,

$$\sum_{j=1}^{N} \int_{\Omega} \varphi_i \varphi_j \, d\Omega \, (\nabla u_h^{\star})_j = \int_{\Omega} \varphi_i \, d\Omega \, (\nabla u_h^*)_i \quad i = 1, \ldots, N, \quad (11)$$

where $(\nabla u_h^*)_i$ are the nodal values of $\nabla \mathbf{u}^*$. Finally, we define the new local error estimator, referred to as the spatial error estimator (SEE):

$$\xi_e = \frac{\| \nabla u_h^{\star} - \nabla u_h^* \|_{L_2(e)}}{\| \nabla u_h^* \|_{L_2(e)}} . \quad (12)$$

Adaptive mesh refinement

The algorithm for adaptive mesh refinement consists of evaluating the local error estimator in each element, and if it exceeds a tolerance value ($\xi_e > tol_e$), the size of the element is halved. This procedure is iterative, with each iteration k evaluating the mesh, reducing the size of the elements that need refinement, and generating a new mesh $(k+1)$ based on this information. The solutions $\mathbf{u}^k$ and $\mathbf{u}^{k+1}$ are evaluated at positions $(\mathbf{x}^*, \mathbf{y}^*)$, such that the maximum value of the relative difference

$$\max \left(\left| \frac{\mathbf{u}^k(\mathbf{x}^*, \mathbf{y}^*) - \mathbf{u}^{k+1}(\mathbf{x}^*, \mathbf{y}^*)}{\mathbf{u}^{k+1}(\mathbf{x}^*, \mathbf{y}^*)} \right| \right) < tol_u$$

is smaller than the established tolerance criterion (tol_u), then the refinement procedure is terminated. To prevent the elements from being drastically reduced in size, a minimum area value (A_{min}) was adopted.

Results: Poisson's equation

Figure 6 shows the results using BEE and SEE refinements in Poisson's equation. The spatial derivatives have values close to those obtained analytically, with a relative error of less than 1% (Figure 7). The main difference between these results is the direction of the refinement region around the positions $(\mathbf{x}^*, \mathbf{y}^*)$ for the SEE refinement, which results in a mesh with fewer nodes (1915 nodes) compared to the BEE refinement (2158 nodes). The difference in the number of nodes between the meshes is small, but it is an indication that the SEE refinement does not refine the entire mesh as in the BEE refinement.

Results: magnetotelluric method

We applied the refinement procedures to a larger problem, in this case, the modeling of the MT method. We will address the 2D modeling, defined by the variation of the isotropic electrical conductivity (σ) only in the (x,z) plane. The total fields **E** and **H** are defined as the sum of primary and secondary fields (Hohmann, 1987). Thus, the electric component in the strike direction (y direction), transverse

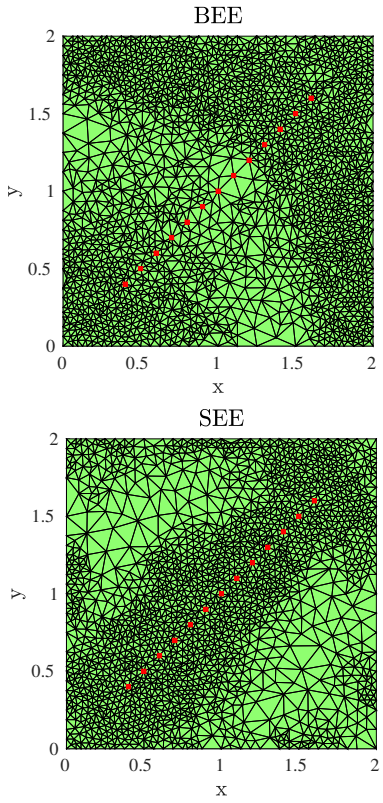

Figure 6 – Meshes obtained with BEE and SEE refinements. The values at the red points are plotted in Figure 7.

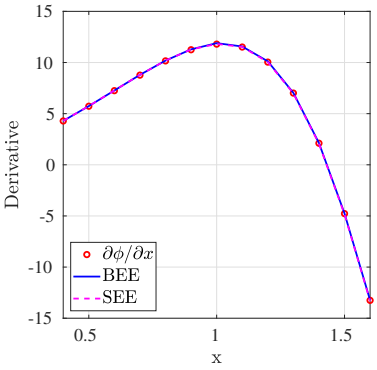

Figure 7 – Profile with the values of spatial derivatives at positions $(\mathbf{x}^*, \mathbf{y}^*)$, obtained with the meshes from Figure 6.

electric mode (TE), is obtained by the equation.

$$\nabla \cdot \left(\frac{1}{\mathfrak{z}} \nabla E_y^s \right) - \sigma E_y^s = J_y^s , \quad (13)$$

where $\mathfrak{z} = i\omega\mu_0$ is the impedance and $J_y^s = \Delta\sigma E_y^p$ is the current density. To calculate the apparent resistivity and phase, it is necessary to obtain the component H_x^s, which

is obtained by taking the derivative,

$$H_x^s = \frac{1}{\imath\omega}\frac{\partial E_y^s}{\partial z}. \quad (14)$$

The validation of the MT modeling is performed using a 1D model, which consists of a layer with a thickness of 500 m inserted into a homogeneous half-space at a depth of 1000 m. The conductivity of the layer and the half-space is 10^{-2} and 10^{-3} S/m, respectively. The MT sounding is conducted with frequencies ranging from 10^{-3} to 10^{3} Hz.

The refinement procedure is applied on the same mesh for each frequency, starting from the lowest frequency up to the highest. In addition, to optimize the process, the target area is reduced, which is limited by a region that depends on the skin depth of each frequency.

Figure 8 shows the result using SEE refinement, where the refinement region is directed around the observation point, generating a mesh with 19074 nodes. In contrast, in the BEE refinement, the heterogeneity is the target of the refinement, which generates a mesh with 76578 nodes. The apparent resistivity and phase values obtained with these two meshes are very close to the 1D modeling results, with a relative error of less than 0.4% (Figure 9).

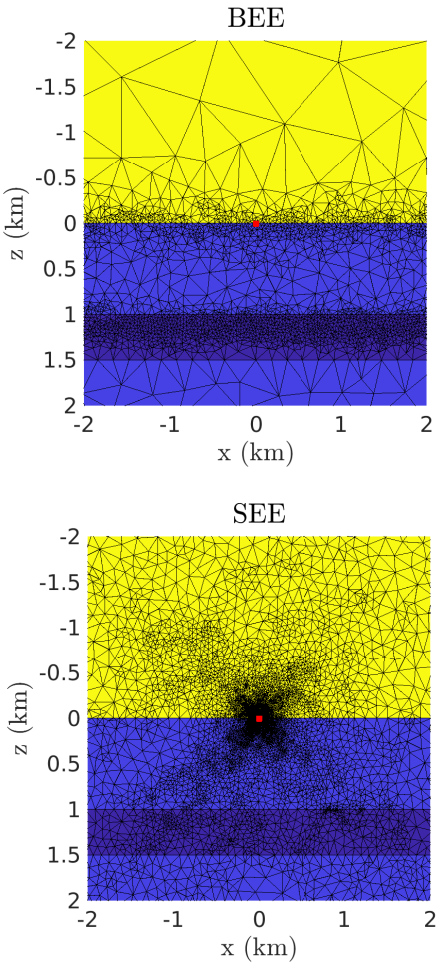

Figure 8 – Meshes obtained with BEE and SEE refinements. The MT sounding is performed at the red point.

Conclusion

We present a new approach to calculate the spatial derivatives of solutions using FEM. In the literature, there are several numerical methods to compute these components; however, we propose a semi-analytical approach. We validated this procedure in a small and easy-to-visualize problem (Poisson's equation), where the solution and derivatives are obtained analytically. Furthermore, we present a particular case in which the spatial derivatives are calculated at specific coordinates of the mesh discretization, generating a modified gradient of the solution. This gradient is used in the recovery-based error estimation method, and then the spatial error estimator (SEE) is formulated. The mesh obtained in the SEE refinement presents a higher refinement around the positions of interest, similar to the results obtained with dual error estimators. However, the proposed estimator is much simpler to apply and more efficient because it does not require an adjoint solution of the finite element system.

The SEE refinement procedure is applied to the 2D modeling of the MT method, resulting in a mesh that is four times smaller than the one obtained with the BEE refinement. In this case, a mesh undergoes the refinement process for each frequency. The process is optimized by targeting the refinement area based on the skin depth, meaning that the refinement area decreases as the frequency increases. This approach enables the generation of EM fields accurately across the entire frequency range.

In conclusion, we have presented the application of the semi-analytic spatial derivative in adaptive mesh refinement and in the calculation of the magnetic component in the MT method. These two applications are important in electromagnetic methods, as it is necessary to obtain a mesh that generates the lowest possible error in modeling and inversion processes. Depending on the problem formulation, it is also necessary to obtain the components of the EM field through spatial derivatives.

References

Ainsworth, M. & Oden, J., 2000. A Posteriori Error Estimation in Finite Element Analysis, Pure and Applied Mathematics: A Wiley Series of Texts, Monographs and Tracts, Wiley.

Grätsch, T. & Bathe, K.-J., 2005. A posteriori error estimation techniques in practical finite element analysis, Computers Structures, vol. 83(4): 235–265, doi:https://doi.org/10.1016/j.compstruc.2004.08.011.

Hohmann, G. W., 1987. Electomagnetic Methods in Applied Geophysics, Vol. 1, Theory, Investigations in Geophysics, vol. 1, chapter Numerical Modeling for Electromagnetic Methods of Geophysics, SEG, 312–363.

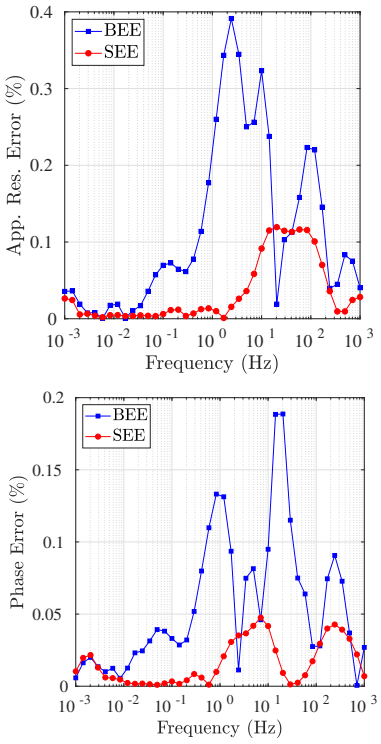

Figure 9 – Profiles with the relative error values of apparent resistivity and phase, obtained with the meshes from Figure 8.

Jin, J., 2002. The Finite Element Method in Electromagnetics, A Wiley-Interscience publication, Wiley.

Key, K. & Ovall, J., 2011. A parallel goal-oriented adaptive finite element method for 2.5-d electromagnetic modelling, Geophysical Journal International, vol. 186(1): 137–154, doi:10.1111/j.1365-246X.2011.05025.x.

Key, K. & Weiss, C., 2006. Adaptive finite-element modeling using unstructured grids: The 2d magnetotelluric example, GEOPHYSICS, vol. 71(6): G291–G299, doi: 10.1190/1.2348091.

Li, Y. & Key, K., 2007. 2d marine controlled-source electromagnetic modeling: Part 1 — an adaptive finite-element algorithm, GEOPHYSICS, vol. 72(2): WA51–WA62, doi:10.1190/1.2432262.

Newman, G. A. & Alumbaugh, D. L., 1997. Three-dimensional massively parallel electromagnetic inversion—I. Theory, Geophysical Journal International, vol. 128(2): 345–354, doi:10.1111/j.1365-246X.1997.tb01559.x.

Zienkiewicz, O. C. & Zhu, J. Z., 1987. A simple error estimator and adaptive procedure for practical engineerng analysis, International Journal for Numerical Methods in Engineering, vol. 24(2): 337–357, doi:https://doi.org/10.1002/nme.1620240206.

Appendix: Galerkin's method

In this appendix, we present the application of the Galerkin method to the Poisson equation (1). The Galerkin method belongs to the family of weighted residual methods, in which the weight functions are equal to the basis functions (Jin, 2002). Let $\mathscr{L}$ be a differential operator, φ_i the weight function, and f the forcing function, then

$$\int_\Omega \varphi_i \mathscr{L}\{\gamma\}^T\{\varphi\}\, d\Omega = \int_\Omega f\ \varphi_i\, d\Omega \quad i = 1,\ldots,N,$$

where γ are the coefficients to be determined. Thus, by applying these integrals to the element e in equation 1,

$$-\int_{\Omega_e} (\nabla\cdot(\nabla\phi))\,\varphi_i\, d\Omega = \int_{\Omega_e} h\ \varphi_i\, d\Omega\,, \tag{15}$$

Applying the vector identity $\alpha\nabla\cdot\mathbf{u} = \nabla\cdot(\alpha\mathbf{u}) - \nabla\alpha\cdot\mathbf{u}$ and the divergence theorem $\int_{\Omega_e}\nabla\cdot\mathbf{v}\ d\Omega = \oint_{\partial\Omega_e}\mathbf{v}\cdot\hat{\mathbf{n}}\ d\Omega$ to the equation above, we obtain,

$$\int_{\Omega_e}(\nabla\phi\cdot\nabla\varphi_i)\ d\Omega = \int_{\Omega_e} h\ \varphi_i\, d\Omega + \oint_{\partial\Omega_e}(\nabla\phi\ \varphi_i)\cdot\hat{\mathbf{n}}\, d\Omega\,, \tag{16}$$

In the equation above, the line integrals on the boundary of each element will cancel out when computed with the contributions from adjacent elements. However, only the components on the domain boundary will remain, where homogeneous Dirichlet conditions are applied. Therefore, the line integral in equation 16 can be neglected.

Writing the electric potential as a linear combination of the basis functions ($\phi = \sum_{j=1}^{3}\phi_j\varphi_j$) and the source term ($h = \sum_{j=1}^{3} h_j\varphi_j$) in equation 16, we have:

$$\sum_{j=1}^{3}\int_{\Omega_e}(\nabla\varphi_j\cdot\nabla\varphi_i)\, d\Omega\ \phi_j = \sum_{j=1}^{3}\int_{\Omega_e}\varphi_j\ \varphi_i\, d\Omega\ h_j\,, \tag{17}$$

with $i,j = 1$ to 3, this is the nodal finite element approximation.

The basis functions are given by $\varphi_i = \frac{1}{2A_e}(a_i + b_i x + c_i z)$, where: $a_i = x_j y_k - x_k y_j$, $b_i = y_j - y_k$ and $c_i = x_k - x_j$, with a cyclic permutation of i, j, and k, and A_e is the area of the element e given by $A_e = \frac{1}{2}\mid a_1 + a_2 + a_3 \mid$.

Solving the integrals in 17 using the formula for polynomial integration on triangles (Jin, 2002; Key & Ovall, 2011), we have:

$$\sum_{j=1}^{3}\left[\frac{1}{4A_e}(b_j b_i + c_j c_i)\right]\phi_j = \frac{A_e}{12}\sum_{j=1}^{3}(1+\delta(i-j))\ h_j\,, \tag{18}$$

where $\delta(i-j)$ is the Dirac delta function. Equation 18 forms the elemental system $\mathbf{K}^e\mathbf{u}^e = \mathbf{g}^e$,

$$K^e_{ij} = \frac{1}{4A_e}(b_j b_i + c_j c_i)\,,$$
$$u^e_i = \phi_i\,,$$
$$g^e_i = \frac{A_e}{12}\sum_{j=1}^{3}(1+\delta(i-j))\ h_j\,,$$

which depend on the vectors $\mathbf{x}^e = [x_1, x_2, x_3]$ and $\mathbf{y}^e = [y_1, y_2, y_3]$.